axis, these harmonics must be transformed to a space-fixed coordinate system before the integrations over the orientations of $\mathbf{R}_i$ and $\mathbf{R}_{i'}$ [*cf.* equation (3)] can be performed. The required transformation is (Rose, 1957)

$$\bar{Y}_{lm'} = \sum_m D^l_{mm'}(\mathbf{R}_{ii'}) Y_{lm} \qquad \text{(A1)}$$

where Y_{lm} is defined in the space-fixed system and where $D^l_{mm'}(\mathbf{R}_{ii'})$ is a Wigner matrix whose arguments are the polar coordinates of $\mathbf{R}_{ii'}$ in the space-fixed frame. The transformed expression for $\langle n(i)n(i')\rangle_T$ may now be plugged into equation (3) together with the Rayleigh expansion of $\exp(-i\mathbf{Q}\,.\,\mathbf{R}_{ii'})$, *i.e.*

$$\exp(-i\mathbf{Q}\,.\,\mathbf{R}_{ii'}) = 4\pi \sum_l (-i)^l j_l(QR_{ii'}) \times \sum_m Y^*_{lm}(\mathbf{R}_{ii'}) Y_{lm}(\mathbf{Q})\,. \qquad \text{(A2)}$$

Integration over the angular coordinates of $\mathbf{R}_i$ and $\mathbf{R}_{i'}$, required by equation (3), may now be performed directly by making use of the rules given in Chapter 4 of Rose (1957).

Integration over the angular coordinates $\mathbf{\Omega}_i$ and $\mathbf{\Omega}_{i'}$ follows a prescription similar to that described above for the angular parts of the $\mathbf{R}_i$ and $\mathbf{R}_{i'}$ integrations. The defining equation [*cf.* equation (3)] for $\alpha_i(\mathbf{Q})$ is first expanded as a Rayleigh series:

$$\alpha_i(\mathbf{Q}) = 4\pi \sum_j a_j \sum_{lm} (-i)^l j_l(Qu_j) Y^*_{lm}(\mathbf{Q}) Y_{lm}(\mathsf{D}_i\,.\,\mathbf{u}_j)\,. \qquad \text{(A3)}$$

In order to introduce the orientational coordinates $\mathbf{\Omega}_i$ of the molecules, the Y_{lm} are rewritten in terms of a set of spherical harmonics, $\tilde{Y}_{lm}(\mathbf{u}_j)$, which are defined in the body coordinate system of a molecule. The required transformation, which is similar to equation (A1), yields:

$$\alpha_i(\mathbf{Q}) = 4\pi \sum_j a_j \sum_{lmm'} (-i)^l j_l(Qu_j) \times Y^*_{lm}(\mathbf{Q}) D^{l*}_{mm'}(\mathbf{\Omega}_i) \tilde{Y}_{lm'}(\mathbf{u}_j) \qquad \text{(A4)}$$

where the argument of the rotation matrix is now the orientation $\mathbf{\Omega}_i$ of the ith molecule. Integrations over $\mathbf{\Omega}_i$ and $\mathbf{\Omega}_{i'}$ may now be carried out and the resulting expressing may be converted to that given by equation (8) by making use of the sum rules for the Clebsch–Gordon coefficients described in Chapter 3 of Rose (1957).

References

BROWN, G. H., DOANE, J. W. & NEFF, V. D. (1971). *A Review of the Structure and Physical Properties of Liquid Crystals.* London: Butterworth.

FAN, C-P. & STEPHEN, M. J. (1970). *Phys. Rev. Lett.* **25**, 500–503.

GENNES, P. G. DE (1971). *Mol. Cryst. Liquid Cryst.* **12**, 193–201.

GENNES, P. G. DE (1972). *C.R. Acad. Sci. Paris, Sér. B*, **274**, 142–148.

MCMILLAN, W. L. (1973). *Phys. Rev.* A**7**, 1673–1678.

PYNN, R. (1973). *J. Phys. Chem. Solids*, **34**, 735–747.

PYNN, R. (1974). *Solid State Commun.* **14**, 29–32.

PYNN, R., OTNES, K. & RISTE, T. (1972). *Solid State Commun.* **11**, 1365–1367.

RISTE, T. & BJERRUM-MØLLER, H. (1975). Private communication and to be published.

RISTE, T. & PYNN, R. (1973). *Solid State Commun.* **12**, 409–412.

ROSE, M. E. (1957). *Elementary Theory of Angular Momentum.* New York: John Wiley.

STINSON, T. W. & LITSTER, J. D. (1970). *Phys. Rev. Lett.* **25**, 503–506.

Acta Cryst. (1975). A**31**, 327

Energy-Dispersive Spectroscopic Methods Applied to X-ray Diffraction in Single Crystals

BY B. BURAS AND J. STAUN OLSEN

Physical Laboratory II, *H. C. Ørsted Institute, University of Copenhagen, DK*-2100 *Copenhagen, Denmark*

AND L. GERWARD, B. SELSMARK AND A. LINDEGAARD ANDERSEN

Laboratory of Applied Physics III, *Building* 307, *Technical University of Denmark, DK*-2800 *Lyngby, Denmark*

(*Received* 1 *October* 1974; *accepted* 25 *December* 1974)

Two single-crystal energy-dispersive crystallographic methods (the fixed-crystal method and the rotating-crystal method) are described and investigated. Formulae for integrated intensities are derived for mosaic and perfect single crystals. Experimental results and a comparison between measured and calculated integrated intensities for a perfect germanium crystal are given. Special features and possible applications of the methods are discussed.

1. Introduction

Energy-dispersive X-ray diffractometry, since it was introduced by Giessen & Gordon (1968) and by Buras, Chwaszczewska, Szarras & Szmid (1968), has been used almost exclusively for studies of powdered crystals. A few results on single-crystal diffraction have been published, dealing with escape peaks (Fukamachi,

Togawa & Hosoya, 1973; Buras, Staun Olsen, Lindegaard Andersen, Gerward & Selsmark, 1974) and polarity (Hosoya & Fukamachi, 1973).

The present paper discusses in some detail the possibilities of energy-dispersive X-ray analysis in single-crystal diffractometry. Two methods, namely the fixed-crystal method and the rotating-crystal method, both proposed by Buras (1971), have been investigated. Formulae for the integrated intensities have been derived for the mosaic crystal as well as for the perfect single crystal. Experimental results and a comparison between measured and calculated integrated intensities for a perfect germanium crystal are given. Finally, special features and possible applications of the methods are discussed.

2. Description of the energy-dispersive spectroscopic methods

2.1. *Fixed-single-crystal method*

In Fig. 1 a collimated polychromatic X-ray beam is scattered from a single-crystal sample, adjusted for reflexion in a particular set of lattice planes.The energy spectrum of the X-rays scattered through a fixed angle, $2\theta_0$, is measured by a semiconductor detector connected to a multichannel pulse-height analyser. Fig. 2 shows an Ewald construction in the reciprocal lattice. One notices that the reciprocal-lattice points corresponding to the recorded reflexions are situated on a straight line (*e.g.* 111, 222, 333, 444, ...). As the energy limits the available wave-vector range to be between $k_{\min}=2\pi E_{\min}/hc$ and $k_{\max}=2\pi E_{\max}/hc$ it will only be the reflexions lying on the line segment of length $2(k_{\max}-k_{\min})\sin\theta_0$ that can be obtained. This is shown in more detail in Fig. 3. Experimental results are presented in § 3.

The relation between the interplanar spacing, d_H, and the corresponding photon energy, E_H, recorded by the multichannel pulse-height analyser is described by the equation (Cole, 1970)

$$E_H d_H \sin\theta_0 = 6{\cdot}199 \text{ (keV Å)}, \qquad (1)$$

where H denotes hkl.

2.2. *Rotating-crystal method*

Imagine the sample shown in Fig. 1 to rotate around an axis perpendicular to the incident beam. The sample consists of a single crystal adjusted to have a suitable zone axis parallel to the axis of rotation. A particular set of lattice planes selects an appropriate wavelength from the incident continuous X-ray spectrum and produces a diffracted beam whenever the crystal is rotated through the reflexion position.* It follows from the Ewald construction that the reciprocal-lattice points corresponding to the zero-layer reflexions are contained within two circles of radius $2k_{\min}\sin\theta_0$ and

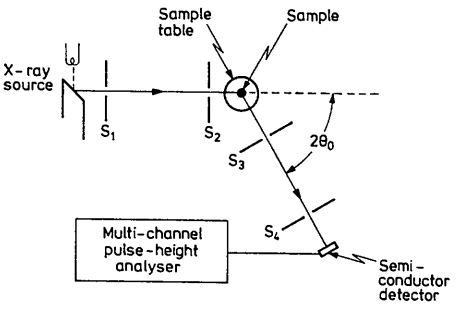

Fig. 1.

Fig. 1. Principle of the energy-dispersive spectroscopic methods. S_1, S_2, S_3 and S_4 slits defining the beam paths.

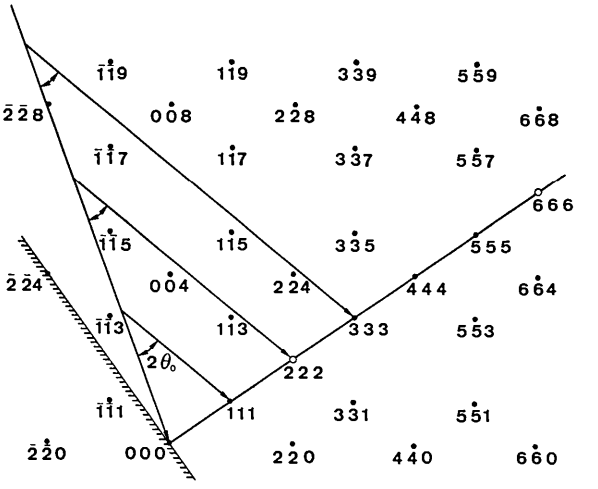

Fig. 2. Ewald construction explaining the fixed-crystal spectroscopic method for a fixed scattering angle in the case of a diamond lattice. The crystal surface is indicated parallel to the (111) planes. Zone axis [1$\bar{1}$0]. Notice the forbidden reflexions 222 and 666, indicated with open circles.

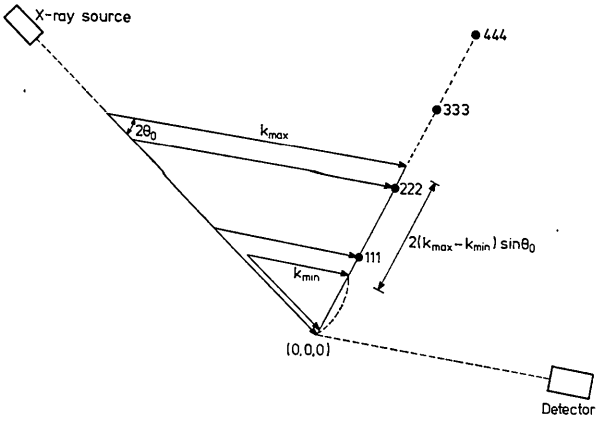

Fig. 3. Ewald construction showing that the recorded reflexions are all confined to the straight-line segment $2(k_{\max}-k_{\min})\sin\theta_0$.

* We restrict ourselves to zero-layer reflexions. However, several layers of reflexions can be recorded simultaneously using a number of detectors.

$2k_{max}\sin\theta_0$, where $2\theta_0$ is the fixed scattering angle. The points are obtained by rotating the line segment $2(k_{max}-k_{min})\sin\theta_0$ (Fig. 3) around an axis passing through (0,0,0). Experimental results are presented in § 3.

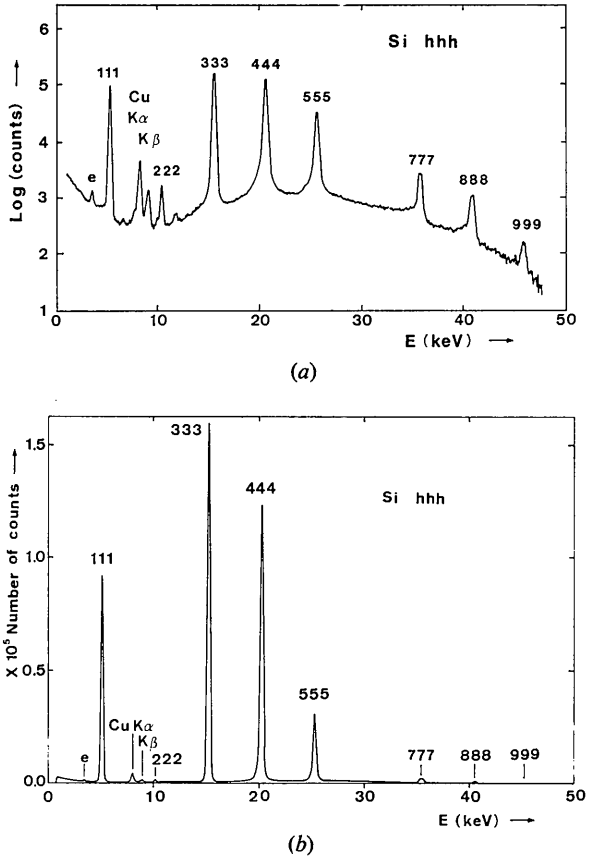

Fig. 4. Diffraction pattern from a fixed single crystal of silicon. $2\theta_0=48°$, *e* silicon escape peak. (*a*) logarithmic scale. (*b*) linear scale. Notice the forbidden reflexion 222.

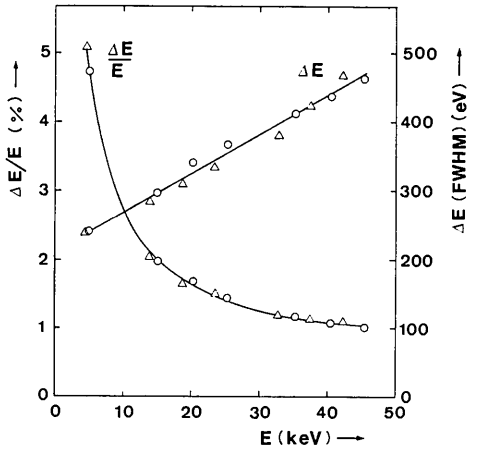

Fig. 5. Experimental resolution of the fixed-crystal method. ΔE full width at half maximum. Circles: silicon diffraction peaks, triangles: germanium diffraction peaks.

3. Experimental results

The experimental arrangement shown in Fig. 1 has been used in the present work. Copper and tungsten diffraction tubes operated between 40 kV and 50 kV have been used as the X-ray source. A collimating system composed of linear slits has been used. The scattered X-rays have been analysed by an Ortec Series 7000 Si(Li) detector connected to a Canberra Model 8100 multichannel pulse-height analyser with 1024 channels. The resolution of the detector is 180 eV FWHM at 5·9 keV. The recorded diffraction peaks have been fitted to Gaussian peaks for the evaluation of peak positions and integrated intensities.

Figs. 4(*a*) and (*b*) show a *hhh* diffraction pattern obtained with the fixed-crystal method using logarithmic and linear scales respectively. The sample is a large perfect silicon crystal, oriented for the symmetric Bragg case of diffraction. The high peak-to-background ratio is to be noticed. The exposure time in this case is relatively small: using a copper tube operating at 50 kV and 14 mA (constant potential) we could easily obtain in 80 s 10000 counts in the 333 peak located at 15 keV and having a resolution of 2%. As can be seen from Fig. 5 the full width at half maximum $|\Delta E_H|$, increases with the increasing photon energy. However, the resolution defined as $|\Delta E/E_H|$ is better in the high energy range, where in our case it approaches 1%.

As can be seen from Fig. 4(*a*) the 222 reflexion from silicon is recorded along with the other reflexions. This reflexion is forbidden in the diamond structure. However, tetrahedral charge distribution of the bonding electrons and anisotropy of the thermal vibrations result in a small non-zero structure factor. The intensities of the forbidden reflexions might be strongly affected by multiple Bragg reflexions. The advantages of the energy-dispersive method for measuring forbidden reflexions are twofold: Firstly the crystal orientation is easily adjusted using the strong reflexions which appear simultaneously. Secondly there is much more freedom in choosing a proper wavelength in order to avoid (or study) multiple-beam diffraction.

Fig. 6 shows some diffraction patterns obtained with the rotating-crystal method. A number of diffraction patterns of silicon and KCl with different axes of rotation have been measured and indexed. The speed of rotation (of the order of 60 r. p. m.) was much higher than in the conventional rotating method. It ensures the simultaneous appearance of all peaks. If this is not important the crystal can be rotated with any desired speed. In principle, it is also possible to correlate the switching on and off of the analyser with the angle of rotation so that only parts of the pattern are recorded. This can be important in special cases.

In the case of both a fixed crystal and a rotating crystal the scattering angle can be chosen in such a way as to ensure the recording of the most important re-

flexions with the optimum intensity and resolutions. When necessary two or more detectors can simultaneously record reflexions at different scattering angles.

4. Formulae for integrated intensities of reflexions

The integrated intensities depend, as is well known, on the state of perfection of the single crystal. Two extreme cases are considered in this section, namely the ideal mosaic crystal (negligible primary and secondary extinction) and the large perfect crystal. In the first case the kinematical theory and in the second the dynamical theory of diffraction are used.

Notation

The notation used here is in the main the same as that of Zachariasen (1945).

h	Planck's constant.
c	Velocity of light.
r_e	Classical electron radius.
λ	X-ray wavelength.
$i_0(\lambda)$	Intensity per unit wavelength range of the incident beam.
$i_0(E)$	Intensity per unit energy range of the incident beam.
S_0	Cross section of the incident beam.
V	Effective crystal volume.
b	Ratio of the direction cosines of the incident and reflected beams relative to normal to surface.
N	Number of unit cells per unit volume.
P_H	Integrated intensity (=total diffracted power).
R_H	Integrated reflexion power.
F_H	Structure factor of index $H(=F'_H+iF''_H)$.
j_H	Multiplicity factor.
K	Polarization factor. $K=1$ for normal component and $K=\|\cos 2\theta_0\|$ for the parallel component.
μ	Linear absorption coefficient.
L_{abs}	Absorption length $(=\mu^{-1})$.
L_{ext}	Extinction length $[=(2KNr_e\lambda\|F'_H\|)^{-1}]$.
$\|g\|$	$=\mu/(2KNr_e\lambda\|F'_H\|)=L_{ext}/L_{abs}$.

4.1. *Ideal mosaic crystal*

4.1.1 *Fixed-crystal*

The total diffracted power in the classical Laue method is given by

$$P^{\text{mosaic}}_{H,\text{fixed}}=i_0(\lambda)V(Nr_e|F_H|)^2\lambda^4\frac{1+\cos^2 2\theta_0}{4\sin^2\theta_0}. \qquad (2)$$

Equation (2) is derived with the assumptions of negligible absorption and extinction and of an unpolarized incident beam.* It is also assumed that $i_0(\lambda)$ is a slowly varying function of λ over the small width of each peak so that the integration can be performed using the value of $i_0(\lambda)$ at the peak position (von Laue, 1960).

* The polarization problem is discussed in connexion with equation (6).

Using

$$i_0(E)=\left|\frac{d\lambda}{dE}\right| i_0(\lambda)=\frac{\lambda^2}{hc}i_0(\lambda)=\frac{hc}{E^2}i_0(\lambda)$$

and the Bragg equation, one can rewrite equation (2) as

$$P^{\text{mosaic}}_{H,\text{fixed}}=hc(Nr_e)^2V[i_0(E)d^2|F|^2]_H(1+\cos^2 2\theta_0)\,. \qquad (3)$$

The subscript H on the right-hand side of equation (3) means that the quantities E, d and F depend on the reflexion hkl.

In structure studies only the knowledge of the relative values of the structure factors are important. Thus for practical purposes the constant factors in equation (3), including the scattering angle, can be omitted.

4.1.2 *Rotating single crystal*

In this section zero-layer reflexions for a fixed scattering angle are considered. The integrated power of a reflexion H is easily obtained by multiplying the corresponding expression for the fixed crystal [equa-

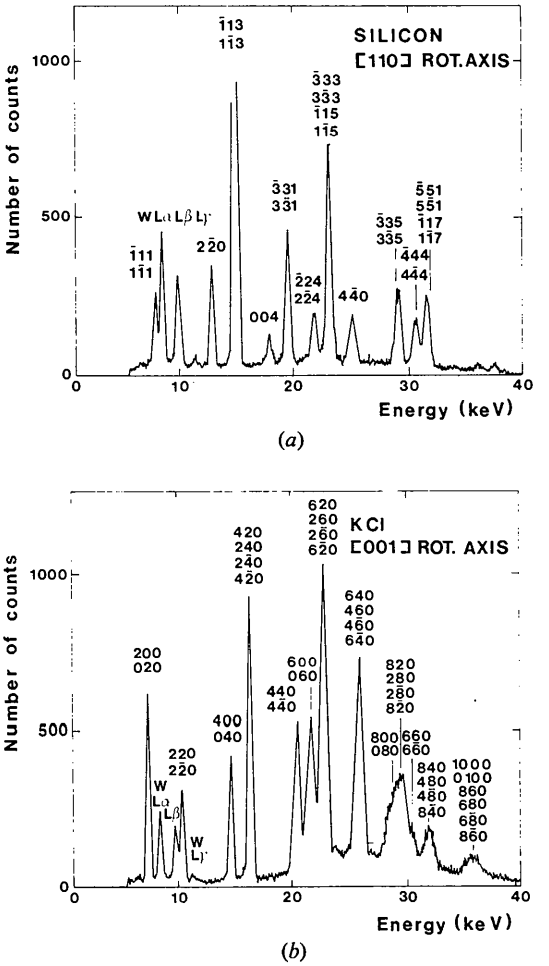

Fig. 6. Diffraction pattern from a rotating single crystal. (*a*) Silicon, axis of rotation parallel to [110]. $2\theta_0=30°$. (*b*) KCl, axis of rotation parallel to [001]. $2\theta_0=32°$.

tion (3)] with a factor $[j_H^{\text{rot}}\Delta\theta_0/(2\pi)]$, where j_H^{rot} is the multiplicity factor of the reflexion H in the crystallographic zone defined by the rotation axis, and $\Delta\theta_0$ is the divergence of the X-ray beam. $\Delta\theta_0/(2\pi)$ is the fraction of time in which a particular set of lattice planes is in a reflexion position. Thus the integrated power is given by

$$P_{H,\text{rot}}^{\text{mosaic}}=hc(Nr_e)^2V[i_0(E)d^2j|F|^2]_H(1+\cos^2 2\theta_0)\frac{\Delta\theta_0}{2\pi}. \quad (4)$$

For practical purposes the constant factors in equation (4) can be omitted [*cf.* equation (3)].

4.2. *Large perfect single crystal*

The rotating-crystal method generally uses small samples and the formulae of the preceding section are valid. Therefore only the case of a *fixed* single crystal is considered in this section. The total diffracted power in the Laue method is given by (Zachariasen, 1945)

$$P_{H,\text{fixed}}^{\text{perfect}}=[R_{H,n}^{\lambda}i_{0,n}(\lambda)+R_{H,p}^{\lambda}i_{0,p}(\lambda)]S_0\,, \quad (5)$$

where R_H^{λ} is the reflexion power integrated on the wavelength scale, and the subscripts n and p indicate that R_H has to be evaluated separately for the normal and parallel components of polarization. The same assumption concerning $i_0(\lambda)$ as in connexion with equation (2) is made here. Zachariasen (1945) has shown that the diffracted power can be calculated in terms of a parameter y, and then converted to an expression in terms of the quantity which is chosen as the independent variable in the actual experiment. The reflexion powers integrated on the wavelength scale and the y scale, respectively, are related by

$$R_H^{\lambda}=\frac{1}{2\pi}|b|^{-1/2}Nr_e\lambda^3|F'_H|\frac{K}{\sin^2\theta_0}R_H^y\,. \quad (6)$$

In the following a symmetric Bragg case of diffraction is considered, *i.e.* $|b|=1$. Furthermore, the incident beam is assumed to be unpolarized,* *i.e.* $i_{0,n}=i_{0,p}=i_0/2$ and one has

$$P_{H,\text{fixed}}^{\text{perfect}}=\frac{hc}{\pi}Nr_eS_0[i_0(E)d|F'|]_H\frac{R_{H,n}^y+|\cos 2\theta_0|R_{H,p}^y}{2\sin\theta_0}. \quad (7)$$

For practical purposes the constant factors in equation (7) can be omitted. R_H^y must generally be calculated by numerical integration but Hirsch & Ramachandran (1950) have developed an empirical formula for a centrosymmetric crystal. It fits the actual values to within 2%:

$$R_H^y=\frac{\pi(1+\kappa^2)}{4\{|g|+\exp[-(1+\kappa^2)^2(|g|+C)]\}}, \quad (8)$$

* The polarization of the Bremsstrahlung from a thick target is in general negligible except for energies very close to the high-energy limit. It affects the diffracted intensities with less than 4% at the scattering angles and the peak positions used in this work (Alstrup, 1974).

where $|g|=\mu/(2KNr_e\lambda|F'_H|)$, $\kappa=F''_H/F'_H$, and $C=\ln(32/3\pi)=1\cdot225$. The parameter $|g|$ describes the importance of extinction and absorption in determining the intensity of reflexion, a small value of $|g|$ denoting a large extinction and *vice versa*.

It is interesting to consider two limiting cases:

(*a*) *No absorption.* In this case $|g|=\kappa=0$ and equation (8) reduces to $R_H^y=\frac{8}{3}$, which is the Darwin solution for a thick non-absorbing crystal. In this case the H- and θ_0-dependent factors are separated in equation (7).

(*b*) *Absorption is the dominating damping process.* In this case $|g|\gg 1$. It can be shown that equation (7) becomes identical with equation (3), where the effective crystal volume, V, is replaced by $S_0/(2\mu)$. This is exactly the expression for a symmetric Bragg reflexion from a thick mosaic crystal with absorption.

4.3. *Corrections*

As in all diffraction methods a number of corrections have to be included when structure factors are to be determined from the measured intensities.

An obvious correction is due to the spectral response of the detector. However, if the same detector is used throughout the experiments one can regard the intensity i_0 in the preceding formulae as an effective intensity as seen by the detector. Problems connected with the effective spectral distribution measurements are discussed in § 5.

Thermal vibration is taken into account by the Debye–Waller factor in the usual way. Anomalous scattering has to be corrected for if any of the diffraction peaks are located at an energy very close to an absorption edge of the sample. Otherwise this correction is small.

The most crucial corrections for the imperfect crystal concern absorption and extinction. The absorption corrections are applied in the same way as in the conventional methods. However, one has to take into account the wavelength dependence of the absorption coefficient when polychromatic X-rays are used. It is a very fortunate fact that absorption and extinction are automatically taken into account by the dynamical diffraction theory for large perfect crystals. Thus the formulae of § 4.2 need no corrections in this case.

5. Spectral distribution of the incident beam

As can be seen from the formulae in § 4 it is necessary to know the spectral intensity distribution, $i_0(E)$, if the energy-dispersive methods are used for structure analysis.

An obvious way to obtain $i_0(E)$ is to perform

(*a*) a direct measurement with the detector situated in the primary beam.

It is also possible to measure the diffracted intensities from a sample with a known structure. This will give the value of $i_0(E)$ at some discrete points.

Two different methods are here possible:

(*b*) a complete diffraction pattern at a particular scattering angle can be measured;

(*c*) one can use a particular diffraction peak and measure its intensity at various scattering angles.

It has been found in this work that the direct measurements are strongly influenced by forward scattering from the slit system and great care should be taken to minimize this effect. In addition it is advisable to test these measurements with either one or both of the two diffraction methods giving values of $i_0(E)$ at some discrete points. In Fig. 7 the direct measured spectrum, combined with method (*b*) is shown. In the direct measured spectrum we notice the Pb $L\alpha$ and $L\beta$ lines coming from the slit system. Also we notice the In $K\alpha$ and $K\beta$ which result from X-ray fluorescense in the material used to form an electrical contact on the surface of the detector (Heath, 1972). The good fit indicates the correctness of the derived formulae.

Method (*b*) has an advantage compared with (*c*), namely that all angle-dependent factors in the intensity formulae are constant. The drawbacks of method (*b*) are that the structure factors and the correction factors for the different reflexions have to be known accurately.

6. Comparison between measured and calculated integrated intensities

In order to test further our formulae we have undertaken a comparison between measured and calculated integrated intensities of the reflexions from a large perfect germanium crystal. The diffraction patterns were recorded with the fixed-crystal method. The intensity distribution of the incident beam, $i_0(E)$, was calculated from the integrated intensities of the corresponding silicon reflexions and taking into account the direct measurement (Fig. 7). The expected intensities of the germanium reflexions were then calculated and compared with the observed values. Formulae for the integrated intensities are given in § 4.2. The parameter $|g|$ is energy dependent and we have found it convenient to express it in terms of absorption and extinction lengths defined in the following way:*

$$L_{abs}=\mu^{-1};$$
$$L_{ext}=(2NKr_e\lambda|F'_H|)^{-1}; \qquad (9)$$
$$|g|=L_{ext}/L_{abs}\,.$$

L_{ext} and L_{abs} have been calculated and plotted as a function of the photon energy (Fig. 8). The actual values of $|g|$ for the different reflexions can be obtained from the diagram. Values of the structure factors have been taken from the calculations by Dawson (1967), values of the absorption coefficients from the measurements by Persson & Efimov (1970) and by Hildebrandt, Stephenson & Wagenfeld (1973).

* It should be noted that extinction lengths can be defined in many ways, differing by some small numerical factor. For example, the Pendellösung period in the symmetric Laue case is L_{ext} in equation (9) multiplied by $2\pi\cos\theta$.

One notices from Fig. 8 that $L_{ext} < L_{abs}$ for all orders of reflexions from silicon in the energy range used in this work. The value of R_H^v has been found to be nearly constant as predicted by the Darwin formula for a perfect nonabsorbing crystal. L_{abs} of germanium is reduced drastically for energies above the K absorption edge (11·10 keV) so that the intensities of the higher-order reflexions tend to those from a mosaic absorbing crystal.

The calculated and observed intensities of the germanium *hhh* reflexions are shown in Table 1. The agreement is very good, giving an R value less than 3%. This shows that the energy-dispersive methods can be used for the determination of structure factors.

Table 1. *Observed and calculated intensities of the hhh reflexions from a perfect germanium crystal*

$2\theta_0=47{\cdot}7°$

H *hhh*	E (keV)	P_H (obs.) (arb. units)	P_H (calc.) (arb. units)	$\lvert\Delta P_H\rvert$ (arb. units)
333	14·06	40·40	39·70	0·70
444	18·80	44·43	45·29	0·86
555	23·48	12·44	12·78	0·34
777	32·86	1·64	1·44	0·20
888	37·54	0·93	0·68	0·25
999	42·18	0·16	0·11	0·05
		100·00	100·00	2·40

7. Discussion

The methods described above are new and not fully developed and thus they do not pretend to be as precise as the well established methods utilizing monochromatic radiation. The energy-dispersive methods have also some features which limits the precision of measurements: the final energy resolution of the detector system, the necessity of measuring the spectral distribu-

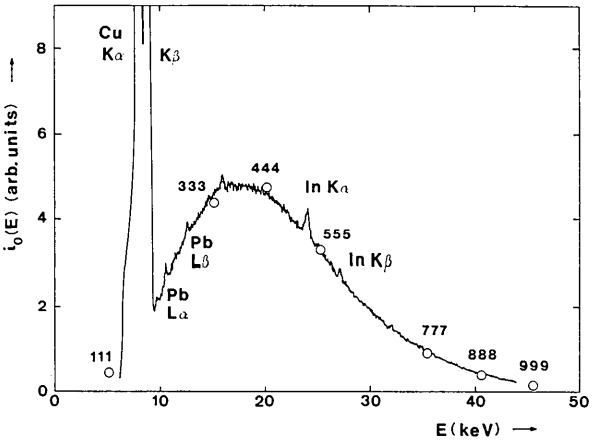

Fig. 7. Spectral distribution of the incident beam. No correction for the detector efficiency has been applied. Copper tube, 50 kV, constant potential. Circles are points calculated from Si *hhh* reflexions using the dynamical theory of diffraction. Full line is measured directly with the detector in the beam.

tion of the incident beam and the wavelength(energy)-dependent absorption.* (The second and third features matter only when integrated intensities are to be measured). However, the energy-dispersive methods have also some special features which might make them useful in certain specific crystallographic studies. The most important future application seems to be in the studies of structure changes (including the kinetics of phase transitions and chemical processes). Here the simultaneous appearance of all reflexions, the short exposure time and the fixed geometry of the experimental set up is of the greatest importance. This is especially true when cryostats, ovens or high pressure devices are used and/or the observed phenomena are time dependent.

* As mentioned previously we are also making an assumption that $i_0(\lambda)$ is a slowly varying function of λ over the small width of each peak.

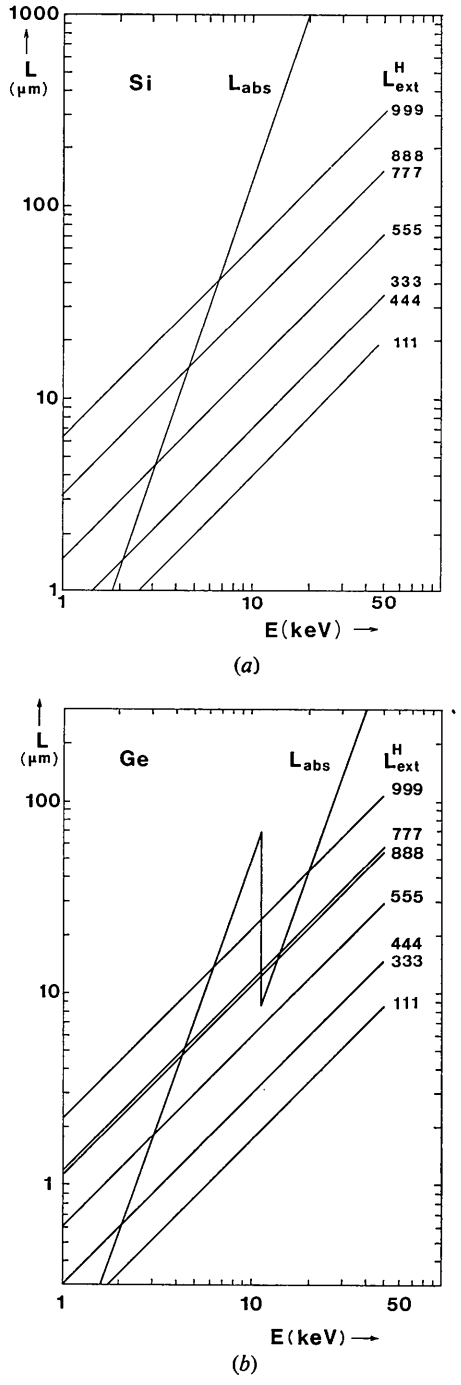

Fig. 8. Extinction and absorption length as function of photon energy. The polarization factor is set to $K=1$. (*a*) Silicon; (*b*) germanium.

The experimental features discussed in § 3 make the fixed-crystal method an interesting alternative when forbidden reflexions are to be measured. The results can be used for the study of anharmonic effects in solids. The methods, especially that of the fixed single-crystal one, could be used for crystal-defect studies, oxidation, and other reactions in thin surface layers. Owing to the different absorption coefficient of X-ray photons associated with different reflexions, different depths of the surface layer can be investigated. It should also be mentioned that an element analysis by means of fluorescence radiation is always simultaneously performed.

The work reported here was made possible by a grant from Statens teknisk-videnskabelige Fond. This financial support is gratefully acknowledged. The authors wish to thank F. Ferrall and B. Ribe for technical assistance.

References

ALSTRUP, O. (1974). Private communication.
BURAS, B. (1971). Monograph 71-08, H. C. Ørsted Institute, Univ. of Copenhagen, Copenhagen.
BURAS, B., CHWASZCZEWSKA, J., SZARRAS, S. & SZMID, Z. (1968). Report 894/II/PS, Institute of Nuclear Research, Warsaw.
BURAS, B., STAUN OLSEN, J., LINDEGAARD ANDERSEN, A., GERWARD, L. & SELSMARK, B. (1974). *J. Appl. Cryst.* **7**, 296–297.
COLE, H. (1970). *J. Appl. Cryst.* **3**, 405–406.
DAWSON, B. (1967). *Proc. Roy. Soc.* A**298**, 379–394, 395–401.
FUKAMACHI, T., TOGAWA, S. & HOSOYA, S. (1973). *J. Appl. Cryst.* **6**, 297–298.
GIESSEN, B. C. & GORDON, G. E. (1968). *Science*, **159**, 973–975.
HEATH, R. L. (1972). *Advanc. X-ray Anal.* **15**, 1–34.
HILDEBRAND, G., STEPHENSON, J. D. & WAGENFELD, H. (1973). *Z. Naturforsch.* **28**a, 588–600.
HIRSCH, P. B. & RAMACHANDRAN, G. N. (1950). *Acta Cryst.* **3**, 187–194.
HOSOYA, S. & FUKAMACHI, T. (1973). *J. Appl. Cryst.* **6**, 396–399.
LAUE, M. VON (1960). *Röntgenstrahl-Interferenzen.* Frankfurt am Main: Akademische Verlagsgesellschaft.
PERSSON, E. & EFIMOV, O. N. (1970). *Phys. stat. sol.* (*a*), **2**, 757–768.
ZACHARIASEN, W. H. (1945). *Theory of X-ray Diffraction in Crystals.* New York: John Wiley.